Periodic-Structure Photoexcitation of a Silicon Coplanar Waveguide for Selective Optoelectronic Microwave Control

WALTER PLATTE

Abstract — **A detailed analysis of the microwave Bragg reflection characteristics of a periodically CW-photoexcited coplanar waveguide on silicon substrate, with special regard to the inherent carrier diffusion mechanisms, is presented. In particular, the carrier diffusion in the direction of wave propagation can strongly affect the stopband reflection spectra of the configuration with respect to magnitude and bandwidth, or efficiency and selectivity, respectively. The dominant effects are studied quantitatively and are outlined in the form of practical performance diagrams. From this, future application of periodically photoexcited transmission line sections for light-induced tunable filters or Bragg reflectors may be inferred. Initial experimental results from a three-section periodic structure of 17 GHz center frequency under 840 nm LED CW excitation are reported.**

I. Introduction

OPTOELECTRONIC control of microwaves has been the subject of considerable interest, particularly in the field of optoelectronic microwave switching [1], [2], where, in most cases, a small laser-pulse-excited region of a semiconductor microstrip or coplanar waveguide affects the switching or gating mechanism. For high-efficiency operation, usually strong irradiances, up to some 10 kW/cm^2 (pulsed), are needed. From this, it is obvious that low-level excitation of some 100 mW/cm^2 from a laser diode or LED yields only poor capability of optoelectronic control. However, when utilizing the distributed Bragg reflection (DBR) characteristics of a finite periodically photoexcited transmission line structure (PPS), e.g. in a semiconductor coplanar waveguide (CPW) as shown in Fig. 1, relatively weakly excited sections can also successfully accomplish certain kinds of optoelectronic control, at least for narrow-band applications.

When cascading the illuminated sections in accordance with the Bragg reflection condition $\Lambda = m(\lambda/2)$ with $m = 1, 2, 3 \cdots$, where Λ is the period of PPS (Fig. 2(a)) and λ is the internal wavelength of the microwave signal to be controlled, the structure acts as a "photoconductivity grating" exhibiting the well-known stopband phenomena [3]. Owing to constructive interference, on the one hand, and light-induced substrate losses, on the other, a total reflection coefficient of up to 40% (at X-band frequencies) can be achieved selectively. Since the period can be changed by altering the illumination pattern (e.g. by means of a pattern-controlled fiber bundle array), a PPS may be developed for light-induced (nonpermanent) tunable filters or tunable distributed Bragg reflectors controlled by pulsed or CW illumination.

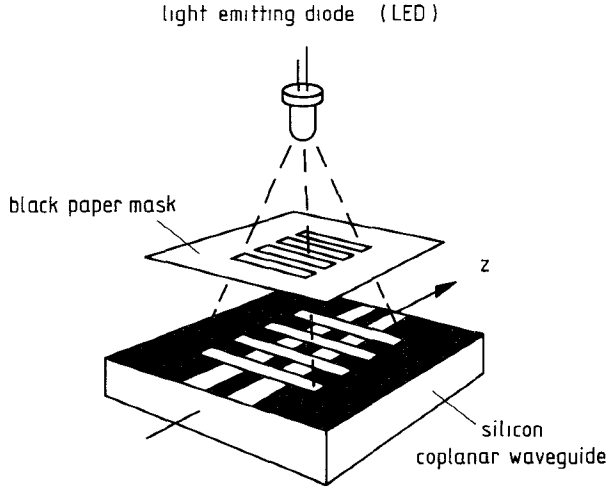

Fig. 1 Principle of periodic-structure photoexcitation.

Operation of PPS under low-level excitation usually implies very small reflections from the excited sections, which simply allows the PPS to be analyzed without considering multiple reflections [4]. Supposing CW illumination, the optically generated excess carriers will diffuse from the excited into the dark sections, thereby causing a diffusion-controlled (nonabrupt) photoconductivity profile in the direction of wave propagation (Fig. 2(b)). This considerably complicates the calculation of total reflection coefficient, compared to the abrupt-profile analysis [5]. In contrast to the light-induced TE-mode DBR structure in a closed-type semiconductor waveguide [6], this quasi-TEM-mode coplanar DBR configuration can be operated by low-power light sources without the need for any heat sinking.

Manuscript received March 15, 1989; revised October 18, 1989
The author is with the Institut fuer Hochfrequenztechnik, Universitaet Erlangen-Nuernberg, Cauerstr. 9, D-8520 Erlangen, West Germany
IEEE Log Number 8934035.

0018-9480/90/0500-0638$01.00

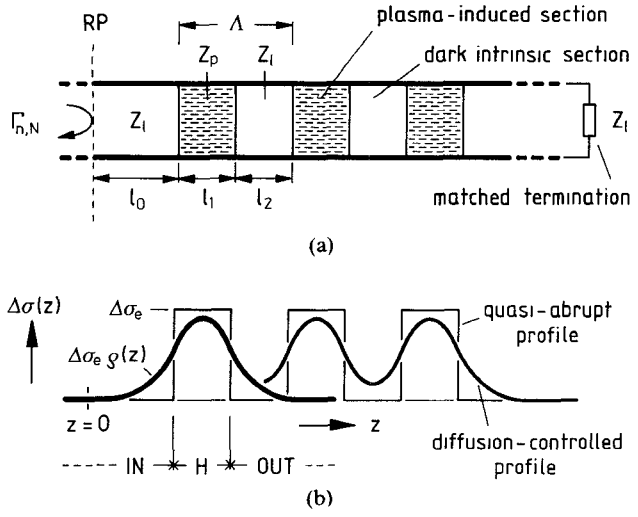

Fig. 2. Periodically photoexcited semiconductor transmission line. (a) Stepped-impedance line model for the analysis. (b) Quasi-abrupt and diffusion-controlled longitudinal photoconductivity profiles $\Delta\sigma(z)$.

II. Analysis of Single Photoexcited Section

A. Propagation Constant and Characteristic Impedance

For a plasma-induced semiconductor CPW in which the major portion of losses is caused by the dominance of shunt conductance per unit length, the attenuation constant α and the phase constant β of the fundamental quasi-TEM mode are approximately given by [7]

$$\alpha = \left\{\left[\left(1+\vartheta_e^2\right)^{1/2}-1\right]^{1/2}\right\}\beta_l/\sqrt{2} \tag{1}$$

$$\beta = \left\{\left[\left(1+\vartheta_e^2\right)^{1/2}+1\right]^{1/2}\right\}\beta_l/\sqrt{2} \tag{2}$$

with

$$\beta_l = \left(\omega^2\mu_0\mu_r\epsilon_0\epsilon_{re}\right)^{1/2} \tag{3}$$

where β_l is the phase constant of a lossless CPW, $\omega = 2\pi f$ with signal frequency f, μ_0 and μ_r are the free-space and relative permeabilities, respectively, ϵ_0 is the free-space permittivity, and ϵ_{re} is the effective dielectric constant of CPW [8]. The quantity ϑ_e is the effective total loss tangent of the substrate covering three loss components (i.e., dielectric, dark-conductivity, and photoconductivity losses [5], [9]) according to

$$\vartheta_e = \frac{\epsilon_r'}{\epsilon_{re}} q_\epsilon \left(\frac{\epsilon_r''}{\epsilon_r'} + \frac{\sigma_d}{\omega\epsilon_0\epsilon_r'} + \frac{\Delta\sigma_e}{\omega\epsilon_0\epsilon_r'} q_p\right) = \vartheta_{e\epsilon} + \vartheta_{ed} + \Delta\vartheta_e \tag{4}$$

where ϵ_r' and ϵ_r'' are the real and imaginary parts of the relative permittivity, q_ϵ is the dielectric filling fraction [8], σ_d is the dark conductivity of the substrate used, and $\Delta\sigma_e$ is the effective CW-induced photoconductivity, which covers the actually inhomogeneous distribution of excess carrier density within any cross-sectional plane of an excited CPW section [9]. It depends on several light-source and substrate parameters (such as optical wavelength, radiation absorption coefficient, relative spectral response of semiconductor material, excess carrier lifetime and mobility, ambipolar diffusion length, surface recombination velocity) as well as on the slot width of CPW [9], [10], and in particular is proportional to the controlling optical power density p. The plasma filling fraction q_p (which is identical to the term s/K used in [9]) denotes the effective plasma-filled portion of the total CPW cross-sectional area loaded with semiconductor material. It also depends on the aforementioned parameters and, in addition, on the characteristic impedance of CPW.

When applying low-level excitation and sufficiently high frequencies, i.e., for $\vartheta_e \ll 1$, (1) reduces to

$$\alpha \simeq \frac{\beta_l\vartheta_e}{2} = \frac{q_\epsilon}{2}\left(\frac{\mu_0\mu_r}{\epsilon_0\epsilon_{re}}\right)^{1/2}\left(\omega\epsilon_0\epsilon_r'' + \sigma_d + q_p\Delta\sigma_e\right)$$

$$= \alpha_\epsilon + \alpha_d + \Delta\alpha \tag{5}$$

exhibiting the contributions of dielectric (α_ϵ), dark-conductivity (α_d), and light-induced losses ($\Delta\alpha$). Likewise, (2) reduces to

$$\beta \simeq \beta_l\left(1+\vartheta_e^2/8\right) \simeq \beta_l. \tag{6}$$

A simple evaluation of (1) and (2) shows that (5) and (6) can be approximately used for $\vartheta_e \leqq 1$ with a relative error of $\leqq 10\%$.

Assuming the dark CPW to have very small losses and, hence, to have a real characteristic impedance Z_l, e.g. $Z_l = 50\ \Omega$ [8], the characteristic impedance Z_p of a plasma-induced CPW may be approximately calculated from [7]

$$Z_p \simeq Z_l\left(1 - j\Delta\vartheta_e\right)^{-1/2} \tag{7}$$

where $\Delta\vartheta_e = q_\epsilon q_p\Delta\sigma_e/\omega\epsilon_0\epsilon_{re}$ from (4).

B. Light-Induced Reflection Coefficient

For the special case of negligible longitudinal carrier diffusion[1], which is characterized by $l_1, l_2 \gg L_a$ [11] (where l_1 and l_2 are the lengths of excited and dark sections, respectively (Fig. 2(a)), and L_a is the ambipolar diffusion length), the light-induced photoconductivity profile $\Delta\sigma(z)$ in the direction of wave propagation z is quasi-abrupt (Fig. 2(b)). Consequently, the PPS may be analyzed by using a stepped-impedance line model [5] where the reflection coefficient Γ_{st} from a single stepped-impedance discontinuity is given by

$$\Gamma_{st} = \frac{Z_p - Z_l}{Z_p + Z_l} \simeq \frac{1-\left(1-j\Delta\vartheta_e\right)^{1/2}}{1+\left(1-j\Delta\vartheta_e\right)^{1/2}} \tag{8}$$

assuming the microwave signal to propagate from the dark into the plasma-induced section. As low-loss excitation with $\Delta\vartheta_e \ll 1$ is assumed to result in $|\Gamma_{st}| \ll 1$, the reflection coefficient Γ_{ss} from a single excited section (i.e., from a pair of discontinuities) may be calculated by summing up only the first-order contributions, according to the

[1]It should be noted that negligible longitudinal carrier diffusion (in the direction of wave propagation) does not necessarily imply negligible carrier diffusion in the transversal direction, and vice versa.

small-reflection theory [4]. Thus, one obtains

$$\Gamma_{ss} \simeq \Gamma_{st}\{1-\exp[-2l_1(\alpha+j\beta)]\}. \quad (9)$$

In general, CW illumination of PPS causes a more or less smoothly broadened (diffusion-controlled) photoconductivity profile $\Delta\sigma_e\rho(z)$ (Fig. 2(b)) where $\rho(z)$ is the relative shape of profile [11]. Provided that the center of the first excited section has been shifted from $z=0$ to $z=l_0+l_1/2$ for practical reasons, where l_0 is the excitation decay length (Fig. 2(b)), $\rho(z)$ of a single excited section can be written as

$$\rho(z)_{IN} = \sinh(l_1/2L_a)\exp[(z-l_0-l_1/2)/L_a], \quad -\infty \leqslant z \leqslant l_0 \quad (10a)$$

$$\rho(z)_{H} = 1-\exp(-l_1/2L_a)\cosh[(z-l_0-l_1/2)/L_a], \quad l_0 \leqslant z \leqslant l_0+l_1 \quad (10b)$$

$$\rho(z)_{OUT} = \sinh(l_1/2L_a)\exp[(-z+l_0+l_1/2)/L_a], \quad l_0+l_1 \leqslant z \leqslant \infty. \quad (10c)$$

Here, the section identification subscripts IN, H, and OUT (from [11]) refer to the input subsection, the high-conductivity subsection, and the output subsection, respectively. In consequence, $\Delta\vartheta_e$, $\Delta\alpha$, and Z_p exhibit diffusion-controlled z dependences which can be obtained by substituting $\Delta\sigma_e \rightarrow \Delta\sigma_e\rho(z)$.

Now, the reflection coefficient Γ_{ss} of a single excited section with diffusion-controlled photoconductivity profile can be determined by summing up all the distributed first-order reflections from the corresponding impedance profile $Z_p(z)$ [4], [12]. Referring to the detailed analysis presented in the Appendix, Γ_{ss-0} in the reference plane at $z=0$ can be expressed as

$$\Gamma_{ss-0} = \Gamma_{IN-0} + \Gamma_{H-0} + \Gamma_{OUT-0} \quad (11)$$

where the three terms of the sum denote the separate contributions of the three subsections according to (A4). A numerical evaluation of (11) for $l_1 \gg L_a$ yields

$$\Gamma_{ss-0}|_{l_1 \gg L_a} = \Gamma_{ss}\exp[-2l_0(\alpha_0+j\beta_l)] \quad (12)$$

where Γ_{ss} is the abrupt-profile reflection coefficient at $z=l_0$ according to (9), and α_0 is the attenuation constant of the dark CPW, i.e., $\alpha_0=\alpha_\epsilon+\alpha_d$.

The typical reflection characteristic $|\Gamma_{ss-0}(\Phi)|$ of a single photoexcited CPW section is shown in Fig. 3, where the signal frequency f has been replaced by the normalized frequency Φ according to $\Phi=2\beta_l l_1$. A qualitative insight into its essential behavior may be obtained as follows: When imagining that $\alpha=0$, $l_0=0$, $l_1 \gg L_a$, and Γ_{st} is not a function of frequency (e.g., $\Gamma_{st}=|\Gamma_{st}(10\text{ GHz})|=0.03=$ const.), $|\Gamma_{ss-0}(\Phi)|$ exhibits a sinusoidal shape within the main frequency range $0 \leqq \Phi \leqq 2\pi$ (curve *1*). Its maximum occurs at $\Phi=\pi$, which corresponds to $l_1=\lambda_q/4$, where λ_q is the internal wavelength of the so-called quarter-wave frequency f_q (see Section III). Next, letting $\alpha \neq 0$ leads to a quasi-sinusoidal shape (curve *2*) with nonzero magnitude at $\Phi=0$ and $\Phi=2\pi$. Then, taking account of the frequency dependence of Γ_{st} from (8) according to $\Delta\vartheta_e \propto 1/\omega$

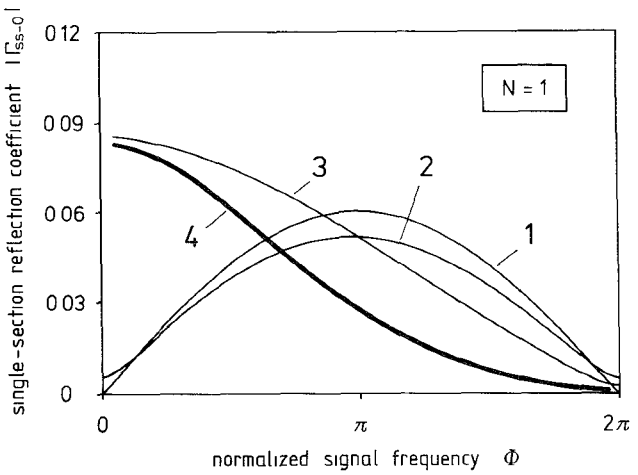

Fig. 3. Evolution of reflection characteristic of a single photoexcited CPW section. (*1*) Ideal case with $\alpha=0$, $\Gamma_{st}=0.03$ being independent of frequency, and negligible longitudinal carrier diffusion. (*2*) With $\alpha \neq 0$. (*3*) With $\alpha \neq 0$ and frequency-dependent $\Gamma_{st}(f)$. (*4*) Real case with $\alpha \neq 0$, $\Gamma_{st}(f)$, and strong longitudinal carrier diffusion. The curves were calculated for a 50 Ω CPW section on silicon substrate under 840 nm CW excitation by substituting $\tau=10^{-4}$ s, $L_a=470$ μm, $f_q=20$ GHz, $l_0=10L_a$, $l_1=(\pi/20)$ cm, and $p=100$ mW/cm², along with A and B as mentioned in subsection III-B.

results in the typical single-section stepped-impedance characteristic (curve *3*), which is a monotonically decreasing function of frequency within the main range $0 \leqq \Phi \leqq 2\pi$ considered here. Furthermore, strong carrier diffusion effects a significant overall reduction of reflection coefficient (diffusion-controlled characteristic, curve *4*). This is readily understood by noting that strong longitudinal carrier diffusion broadens the photoconductivity profile and, hence, lowers the photoinduced differential change in characteristic impedance, thereby causing smaller distributed reflections.

III. Analysis of Periodically Photoexcited Structure

A. Characterization of Reflection Spectra

In general, cascading of dark and excited sections leads to a longitudinal "hill-and-dale" photoconductivity profile, the shape of which can be changed variously by altering the specific lengths l_1, l_2, and L_a [11]. However, to achieve highly effective grooves (of the induced "photoconductivity grating") for frequency-selective optoelectronic control, the individual single-section profiles must not substantially overlap, resulting in the requirement $l_2 \gtrsim 8L_a$ (Fig. 2(b)).

These circumstances, on the one hand, and the small-reflection situation (i.e., $|\Gamma_{ss-0}| \ll 1$), on the other, now enable one to calculate the total reflection coefficient $\Gamma_{n,N}$ at $z=0$ from a finite PPS (Fig. 2(a)) by summing up again only the first-order contributions of the N individual excited sections [4] according to

$$\Gamma_{n,N} \simeq \Gamma_{ss-0}\sum_{\nu=1}^{N}\exp\{-2(\nu-1)\cdot[(\alpha_0+jB)(l_1+l_2)+Al_1]\} \quad (13)$$

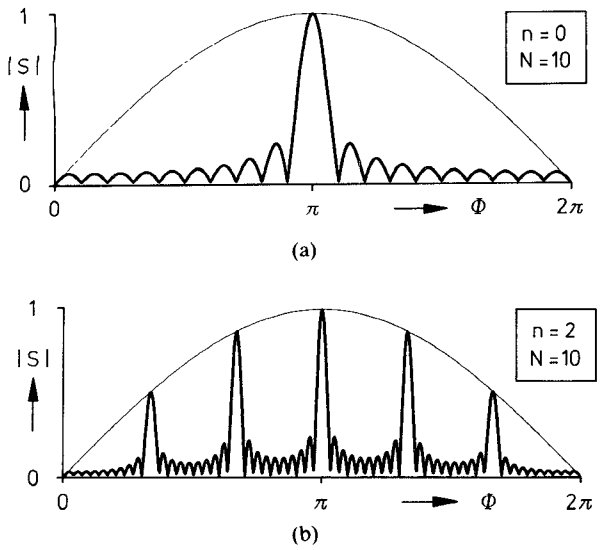

Fig. 4. Illustrative presentation of selectivity term $|S(\Phi)|$ as a function of normalized frequency Φ for the illumination pattern coefficients (a) $n=0$ and (b) $n=2$. The number of excited sections is $N=10$.

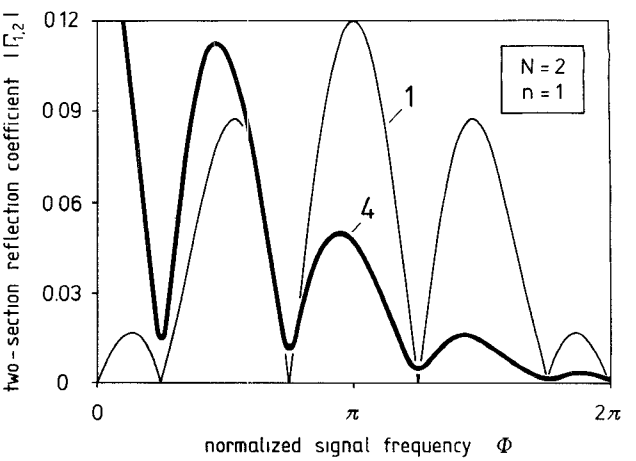

Fig. 5. Typical reflection spectrum of a two-section PPS. (*1*) Ideal characteristic for $\alpha=0$, $\Gamma_{st}=0.03=$ constant, and negligible longitudinal carrier diffusion. (*4*) Diffusion-controlled characteristic for $\alpha\neq 0$, frequency-dependent $\Gamma_{st}(f)$, and strong longitudinal carrier diffusion. The curves refer to the specifications given in the caption of Fig. 3.

where $A=\beta_l\Delta\vartheta_e/2$, $B=\beta_l$, and $\alpha_0=\alpha_\epsilon+\alpha_d$. Maximum signal reflection through constructive interference is then obtained for $l_1=\lambda_q/4$ along with $l_2=(2n+1)l_1$, where $n=0,1,2,3\cdots$, indicating the specific excitation pattern as discussed below. Already incorporated into this equation is the fact that the total light-induced attenuation across a single excited section is Al_1, which is insensitive to the actual shape of photoconductivity profile because of

$$\int_0^{2l_0+l_1}\rho(z)\,dz \simeq \int_{-\infty}^{+\infty}\rho(z)\,dz = l_1 \qquad \text{for } l_0 \gtrsim 4L_a.$$

Moreover, it has been confirmed from a related rigorous analysis that the neglect of return loss and multiple reflections introduces only an error of $\leqq 4\%$ as long as $|\Gamma_{n,N}|\leqq 0.40$ [13].

A qualitative insight into the essential performance of $|\Gamma_{n,N}(\Phi)|$ may be obtained as follows: When imagining again that $\alpha=0$, $l_0=0$, $l_1\gg L_a$, and $l_2\gg L_a$, the magnitude of $\Gamma_{n,N}$ can be written as

$$|\Gamma_{n,N}| \simeq 2\left|\Gamma_{st}\cdot\sin\frac{\Phi}{2}\cdot\frac{\sin N(n+1)\Phi}{\sin(n+1)\Phi}\right| = 2N|\Gamma_{st}S(\Phi)| \tag{14}$$

where $S(\Phi)$ constitutes the frequency-selective behavior of signal reflection as illustrated in Fig. 4, recognizing the $\sin(\Phi/2)$ envelope as curve *1* of Fig. 3. The typical shape of the total reflection spectrum $|\Gamma_{n,N}(\Phi)|$ is then obtained by the weighting of $|S(\Phi)|$ through the frequency dependence of $|\Gamma_{st}(\Phi)|$, resulting in an envelope similar to curve *3* of Fig. 3. For example, Fig. 5 shows the typical reflection characteristics for $N=2$ (with $l_2=3l_1$) in the case of $\alpha=0$, $l_0=0$, $l_1\gg L_a$, $l_2\gg L_a$, and $\Gamma_{st}=0.03=$ constant (curve *1*) as well as in the case of $\alpha\neq 0$ along with strong carrier diffusion and $\Gamma_{st}=\Gamma_{st}(\Phi)$ from (8) (curve *4*).

As anticipated, $|\Gamma_{n,N}|$ is proportional to N, which, of course, holds only for $\alpha=0$ and $|\Gamma_{n,N}|\leqq 0.40$ [13]. For $\alpha\neq 0$ (in particular for $\Delta\alpha\neq 0$) from (13), the contribution of the $(\nu+1)$th excited section to $|\Gamma_{n,N}|$ is reduced because of the attenuation of the ν preceding sections. Thus, the magnitude of each major-lobe reflection coefficient as a function of N actually exhibits sublinear behavior with saturation for $N\to\infty$, resulting in a limiting value $|\Gamma_{n,\infty}|$, as detailed in subsection III-B. Moreover, a numerical evaluation of (13) reveals that the number of excited sections required to produce a total reflection coefficient near $|\Gamma_{n,\infty}|$ strongly decreases with an increase in photoconductivity (i.e., with increasing carrier lifetime and/or increasing irradiance [9]).

It is seen from (14) and Fig. 4 that for $N\gg 1$ the major-lobe maxima appear at $\Phi_q/(n+1)$ or $f_q/(n+1)$, respectively, and those multiples of it which are consistent with constructive interference. From this, diverse illumination patterns may be implied. For example, to operate a PPS for generating maximum reflections at the center frequency f_c, the choice $f_q=f_c$ along with $l_1=l_2=\lambda_q/4$ corresponds to a symmetric excitation pattern ($n=0$, Fig. 6(a)). Another choice is $f_q=2f_c$ along with $l_1=\lambda_q/4$ and $l_2=3l_1$ ($n=1$, Fig. 6(b)), or $f_q=3f_c$ along with $l_1=\lambda_q/4$ and $l_2=5l_1$ ($n=2$, Fig. 6(c)). These latter illumination patterns are desirable from the viewpoint of realizing a better figure of merit (see subsection III-B and Figs. 7 and 8) and saving energy of illumination [5]. The resultant reflection spectra for $N=10$ are recorded in Fig. 6 as well. It is seen, for example, that although the illuminated area of the 1,10 structure is reduced to half of that needed for the 0,10 structure, $|\Gamma_{1,10}|$ is not reduced to half of $|\Gamma_{0,10}|$. Hence, the 1,10 structure proves to work more effectively.

B. Figure of Merit of PPS

Numerical evaluation of (13) also reveals that all the minor lobes which appear for $N\gg 1$ become more and more indistinct with an increase in optically induced attenuation, finally resulting in a single left-hand minimum at $0.5f_c$ and a single right-hand minimum at $1.5f_c$, each with

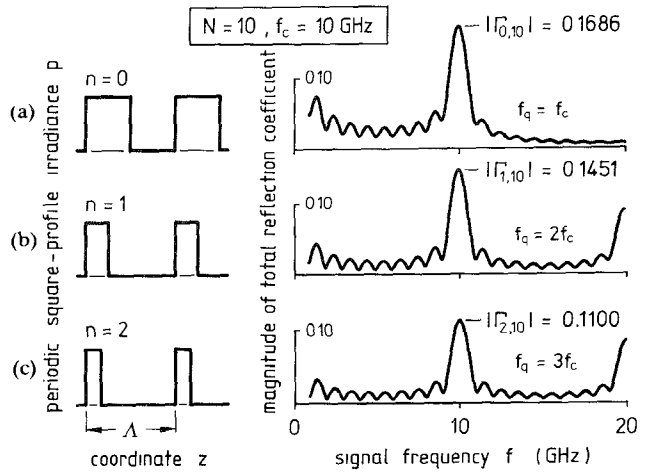

Fig. 6. Various kinds of periodic illumination and the resultant reflection spectra for $N=10$ and (a) $n=0$, (b) $n=1$, and (c) $n=2$. The curves refer to a 50 Ω CPW on silicon substrate under 840 nm CW excitation along with $\tau=10^{-6}$ s, $L_a=47$ μm, $p=345$ mW/cm^2, and $f_c=10$ GHz.

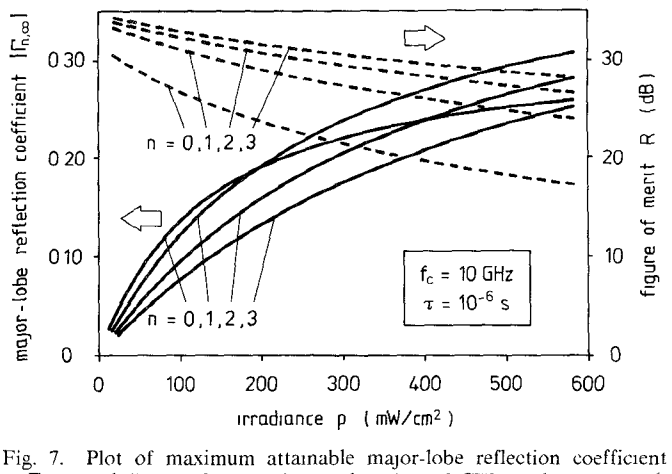

Fig. 7. Plot of maximum attainable major-lobe reflection coefficient $|\Gamma_{n,\infty}|$ and figure of merit R as a function of CW irradiance p with illumination pattern coefficient n as parameter in the case of negligible longitudinal carrier diffusion, at the center frequency $f_c=10$ GHz.

respect to the major-lobe maximum at f_c. Since, on the one hand, the major-lobe reflection coefficient $|\Gamma_{n,N}(f_c)|$ as well as the minimum reflection coefficients $|\Gamma_{n,N}(0.5f_c)|$ and $|\Gamma_{n,N}(1.5f_c)|$ strongly depends on irradiance p and illumination pattern coefficient n, and, on the other hand, the ratio $|\Gamma_{n,N}(f_c)|/|\Gamma_{n,N}(0.5f_c)|$ is a relevant filter parameter (where $|\Gamma_{n,N}(1.5f_c)|$ is lower than $|\Gamma_{n,N}(0.5f_c)|$ and, hence, is less important), it is quite useful to estimate the reflection performance from the aforementioned ratio for $N\to\infty$ by varying p and n. Hence, the figure of merit of a PPS may be defined as the logarithmic ratio R according to

$$R=20\log|\Gamma_{n,\infty}(f_c)/\Gamma_{n,\infty}(f_c/2)|. \tag{15}$$

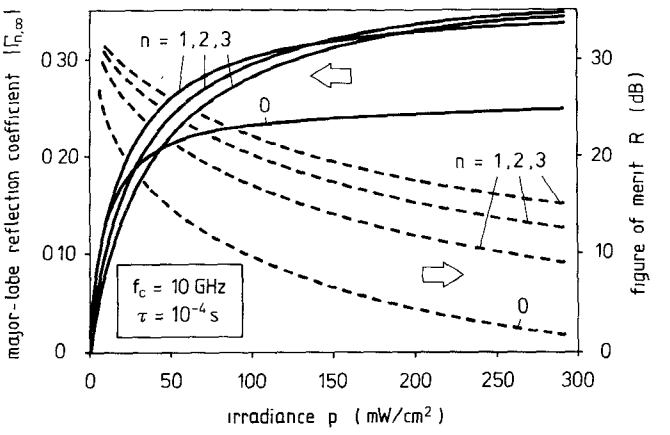

Fig. 8. Plot of maximum attainable major-lobe reflection coefficient $|\Gamma_{n,\infty}|$ and figure of merit R as a function of CW irradiance p with illumination pattern coefficient n as parameter in the case of strong longitudinal carrier diffusion, at the center frequency $f_c=10$ GHz.

Noting that $\sum_{\nu=1}^{\infty}x^{\nu-1}=(1-x)^{-1}$ and $\sum_{\nu=1}^{\infty}(-x)^{\nu-1}=(1+x)^{-1}$, the limiting values $|\Gamma_{n,\infty}|$ can be readily obtained from (13) as

$$|\Gamma_{n,\infty}(f_c)|=|\Gamma_{ss-0}|\{1-\exp[-2\alpha_0(l_1+l_2)-2Al_1]\}^{-1} \tag{16}$$

where $\Gamma_{ss-0}=\Gamma_{ss-0}(f_c)$ and $\alpha_0=\alpha_0(f_c)$, and

$$|\Gamma_{n,\infty}(f_c/2)|=|\Gamma_{ss-0}|\{1+\exp[-2\alpha_0(l_1+l_2)-2Al_1]\}^{-1} \tag{17}$$

where $\Gamma_{ss-0}=\Gamma_{ss-0}(0.5f_c)$ and $\alpha_0=\alpha_0(0.5f_c)$.

As a result, Figs. 7 and 8 show typical plots of $|\Gamma_{n,\infty}(f_c)|$ and R as a function of p with n as parameter. The curves refer to a 50 Ω CPW on silicon substrate of carrier lifetime $\tau=10^{-6}$ s (Fig. 7) and $\tau=10^{-4}$ s (Fig. 8) under 840 nm CW illumination [9], [14]. Further, assuming $q_\epsilon=0.5$ [8] yields B/rad cm$^{-1}\simeq 0.5f$/GHz, assuming $q_p(\tau=10^{-6}$ s$)=0.08$ [9] yields A/Np cm$^{-1}\simeq 4.35\cdot10^{-4}p$/mW cm^{-2}, and assuming $q_p(\tau=10^{-4}$ s$)=0.20$ [9] yields A/Np cm$^{-1}\simeq 6\cdot10^{-3}p$/mW cm^{-2}. Moreover, α_0/Np cm$^{-1}\simeq 3\cdot10^{-3}f$/GHz has been used [5], [14]. As $f_c=10$ GHz has been chosen for example, l_1/cm $=\pi/10(n+1)$ is obtained.

It is seen that $|\Gamma_{n,\infty}|$ increases and R decreases with a rise of irradiance. As anticipated, the higher τ substrate works more effectively. For example, it can produce reflection coefficients of about 0.30 at $p\simeq 100$ mW/cm^2, whereas the lower τ substrate needs 600 mW/cm^2 to attain the same reflections. Further, higher carrier lifetimes cause a more distinct saturation and a reduction of R. Of course, a better figure of merit is obtained with higher n. Moreover, noting that the curves of Fig. 7 agree with those shown in [5, fig. 3], the diffusion-controlled-profile analysis presented here proves to be valid up to the limiting case of negligible longitudinal carrier diffusion.

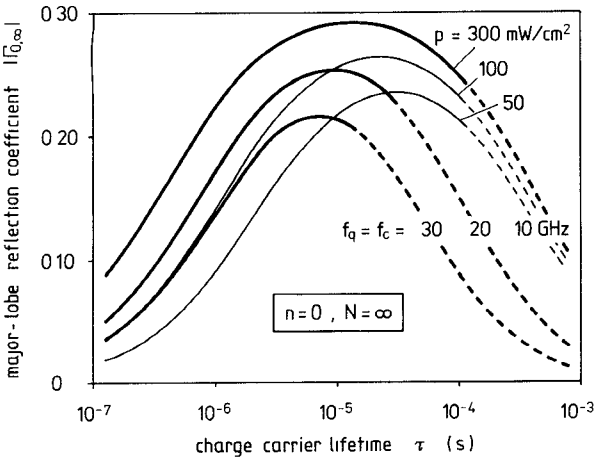

Fig. 9. Plot of maximum attainable major-lobe reflection coefficient $|\Gamma_{0,\infty}|$ as a function of charge carrier lifetime τ with center frequency f_c and CW irradiance p as parameters. The broken curves indicate reduced accuracy due to the actually existing (but disregarded) overlapping of the individual single-section profiles in this range of carrier lifetimes.

IV. Optimum Carrier Lifetime

Bearing in mind the increase of $\Delta\sigma_e$ (and, thus, of $\Delta\vartheta_e$ too) as well as the increase of L_a with rising τ [9], it can be readily understood that the characteristic behavior of $|\Gamma_{n,\infty}(f_c)|$ as a function of τ is governed by two physical effects which are oppositely directed and become dominant one after another: In the low-lifetime range, $|\Gamma_{n,\infty}(f_c)|$ will rise with growing τ due to the increase of differential reflection coefficient $d\Gamma$ (see the Appendix) with growing $\Delta\vartheta_e$ or τ, respectively. On the other hand, photoinduced wave attenuation and carrier diffusion become dominant with a further increase of τ. Hence, in the high-lifetime range, $|\Gamma_{n,\infty}(f_c)|$ is expected to decrease with growing τ due to strong dissipation and, in addition, to the reduction of $d\Gamma$ as a result of diffusion-controlled broadening of the photoconductivity profile.

To be more specific, it should be noted that $\Delta\vartheta_e$ and $\Delta\alpha$ are proportional to q_p, where q_p itself depends on τ and $L_a(\tau)$ via the normalized plasma penetration depth $\delta(\tau, L_a)$ [9]. Moreover, q_p exhibits a second-order dependence on the maximum conductivity contrast ratio ν_m, where ν_m itself is a function of τ via $\Delta\sigma_e(\tau)$ [9]. Considering all the aforementioned relationships, $|\Gamma_{n,\infty}(f_c)|$ as a function of τ can be calculated from (16). As a result, Fig. 9 shows some typical curves, e.g. for $n = 0$ (i.e., $f_q = f_c$, and $l_1 = l_2$), with f_c and p as parameters, referring again to a 50 Ω CPW configuration on silicon substrate under 840 nm CW illumination [9], [14]. It is seen that the total reflection coefficient passes a maximum with growing τ. Thus, it is quite consistent to take the τ value that produces maximum $|\Gamma_{0,\infty}(f_c)|$ as the optimum carrier lifetime. Obviously it exhibits a slight dependence on f_c and p. Nevertheless, when applying silicon substrates under CW excitation up to roughly 300 mW/cm² along with center frequencies up to about 30 GHz, an optimum carrier lifetime of about 10^{-5} s can be inferred from Fig. 9. The broken curves indicate that undesirable overlapping of the single-section profiles [11] can occur in the high-lifetime range. This will affect the total reflection coefficient, which, however, has not been considered in this approach.

V. Experimental Results

Preliminary experimental investigations of PPS were performed with a 50 Ω CPW transmission line on silicon substrate ($\tau = 1$ μs) under 840 nm CW excitation where the controlling radiation from six 50 mW LED's was guided through a shape-changing fiber bundle configuration for uniform illumination of the two slots of CPW [9]. Periodic-structure photoexcitation was then attained by means of a 200-μm-thick overlay film mask on top of the substrate. As the actually usable length of the test CPW was only 10 mm [14] and the automatic network analyzer used was applicable up to 18 GHz, the experiments could only be carried out with a trisection mask ($n = 0$, $N = 3$), producing $l_1 = l_2 = 2$ mm [15]. From this aspect, the experimental results presented here may only be considered a verification of the principle of operation.

For the measurement of the light-induced total reflection spectrum $|\Gamma_{0,3}(f)|$, the PPS was mounted in a special test fixture [9], [14] and connected to the network analyzer at one end of the CPW (port 1) and terminated in a 50 Ω load at the other end (port 2). The molding head (in which the fiber ends were aligned and fixed by epoxy resin) was positioned with its shortest possible distance to the substrate, given by the 200 μm thickness of the film mask. In this way, an irradiance of 315 mW/cm² was produced at the semiconductor surface [14].

In a first (error-correcting) procedure, the input reflection coefficient at port 1 under dark-CPW condition was measured. This quantity usually arises from slight differences between the actual characteristic line impedance and the 50 Ω load as well as from imperfect CPW-to-coaxial adapters. Likewise, in a second procedure, the input reflection coefficient under the periodic-excitation condition was measured. As this latter quantity may approximately be considered the vector sum of the dark-CPW reflection coefficient and the optically induced portion to be determined, the (net) PPS reflection spectrum is then simply obtained from a vector subtraction procedure. As a result, Fig. 10 shows the measured PPS spectrum $|\Gamma_{0,3}(f)|$ where the upper spectrum range from 12.4 to 18 GHz had to be performed without error correction [15]. For comparison, the computed (light-induced) reflection spectrum in the case of perfectly matched termination has been recorded in Fig. 10 as solid curve, where the broken part of it indicates decreasing accuracy due to violation of the low-loss condition in this frequency range for the given parameter constellation.

As the actual substrate thickness was not really infinite [9], [14], the computation was based on a modified B value, namely $B/\text{rad cm}^{-1} = 0.4527\, f/\text{GHz}$ [8], instead of the infinite-thickness B value mentioned in subsection III-B. Nevertheless, the measured spectrum exhibits a slight frequency shift (of the second minimum) toward higher frequencies and, in addition, reveals two distinct "dents"

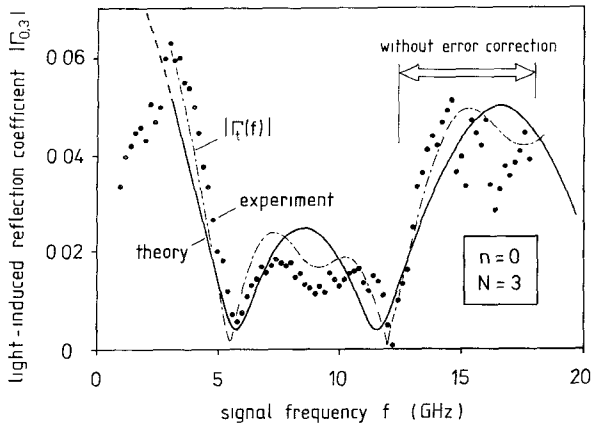

Fig. 10. Light-induced reflection coefficient $|\Gamma_{0,3}|$ of test PPS on silicon substrate versus signal frequency f for the following parameter constellation: CW excitation at 840 nm, $p = 315$ mW/cm^2, $\tau = 1$ μs, $l_1 = l_2 = 2$ mm, $f_q = 17.3$ GHz. For comparison, the dash-dotted curve represents the computed total input reflection spectrum $|\Gamma_t(f)|$ at port 1 as a superposition of the light-induced reflection spectrum $|\Gamma_{0,3}(f)|$ and an undesired portion from the nonzero reflection coefficient at port 2, chosen to be $0.05 \exp(-130^0)$ in this case.

ranging from 7 to 10 GHz and from 15 to 18 GHz. There are three reasons for these effects. First, the phase constant of the CPW under test was influenced by the dielectric material above the substrate, i.e., the polyester mask ($\epsilon_r' \simeq 3.2$) and the molding head ($\epsilon_r' \simeq 3.4$), which has not been incorporated into the analysis. Second, the irradiance across the illuminated sections was actually inhomogeneous because of fiber breakage from experimental manipulations, thereby producing a "subspectrum" which was superposed to the main spectrum inferred from l_1 and l_2 [15]. Third, the determination of light-induced reflection coefficients by the simple subtraction procedure mentioned above is prone to experimental error, because the transformation of signal reflections from the port 2 adapter to the measuring plane at the input adapter (port 1) under the dark-CPW condition is different from that under the excitation condition. It is due to the photosensitivity of the propagation constant of semiconductor CPW. This latter source of error is a typical handicap to any measurement of optically induced reflection coefficients [16] and hardly seems capable of being eliminated. To emphasize this aspect, Fig. 10 also shows the computed total input (port 1) reflection spectrum $|\Gamma_t(f)|$ as a superposition of the light-induced reflection spectrum $|\Gamma_{0,3}(f)|$ and an undesired portion from the nonzero reflection coefficient at the port 2 adapter, which in this case has been chosen $0.05 \exp(-130^0)$ with the assumption of being independent of frequency for simplicity [15].

VI. Concluding Remarks

Analysis and results presented here are based on the assumption that a purely dielectric quasi-TEM mode is propagating on the CPW under a low-loss excitation condition. From this, proper operation of PPS within the frequency range 1–20 GHz along with irradiances up to 300 mW/cm^2 may be implied [9].

Referring to the reduction of the total reflection coefficient (and, hence, of the effectiveness) with increase of f_c, it should be noted that this inherent behavior of a PPS can be compensated to a certain degree by the effect whereby l_1 also decreases with growing f_c; consequently, the optical energy saved may be used for the excitation of another section. Thus, considering the optical energy to be arbitrarily distributable, the number of signal reflections per unit irradiance (i.e., the overall efficiency) becomes much less sensitive to f_c. Moreover, it is seen that the dimensional design of a PPS is not only governed by the relationship between l_1 and f_q but also is subject to the need for generating a truly efficient profile of photoconductivity according to $l_1, l_2 \gtrsim 4L_a$ [11].

Although somewhat incorrect, the neglect of conductor losses against the substrate losses [7], [9] has proved to be a useful assumption to make the analysis of PPS much less complicated. This approach has finally resulted in the simple and clear separation of the substrate loss components according to (5). For (at least approximate) incorporation of conductor losses (α_c) [8] into the theory of PPS, it seems quite consistent to add α_c subsequently in (5), yielding $\alpha = \alpha_c + \alpha_\epsilon + \alpha_d + \Delta\alpha$. This concept already contributes to the numerical results presented here, where the dark-CPW attenuation constant α_0 (subsection III-B) has been assumed to include the conductor losses [14].

In conclusion, it should be noted that the true potential of PPS for optoelectronic microwave control can only be exhausted when applying smaller (optimized [9]) CPW dimensions in conjunction with an adapted pattern-controlled fiber bundle configuration for optimal utilization of the available optical power. As an illustrative example, Fig. 11 shows a sketch of the prototype of coplanar PPS on silicon substrate with a pattern-controlled LED-fed fiber bundle array on top of the CPW which is being realized and tested in the author's laboratory.

Concerning the inherently small light-induced reflection coefficients of magnitudes hardly exceeding 50% (which could be a certain drawback in view of future applications), the effectiveness of PPS can be successfully improved by means of standard microwave circuitry in most cases of interest. Corresponding investigations are currently in progress.

Appendix
Calculation of Diffusion-Controlled Single-Section Reflection Coefficient Γ_{ss-0}

When considering a CPW section with light-induced diffusion-controlled impedance profile $Z_p(z)$ to be made up of a number of sections of line of differential length dz, and for which the characteristic impedance changes by differential amounts dZ from section to section, the step change dZ in impedance at z produces a differential reflection coefficient [4]

$$d\Gamma(z) = \frac{1}{2}\left\{\frac{d}{dz}\left[\ln\frac{Z_p(z)}{Z_l}\right]\right\} dz \qquad \text{(A1)}$$

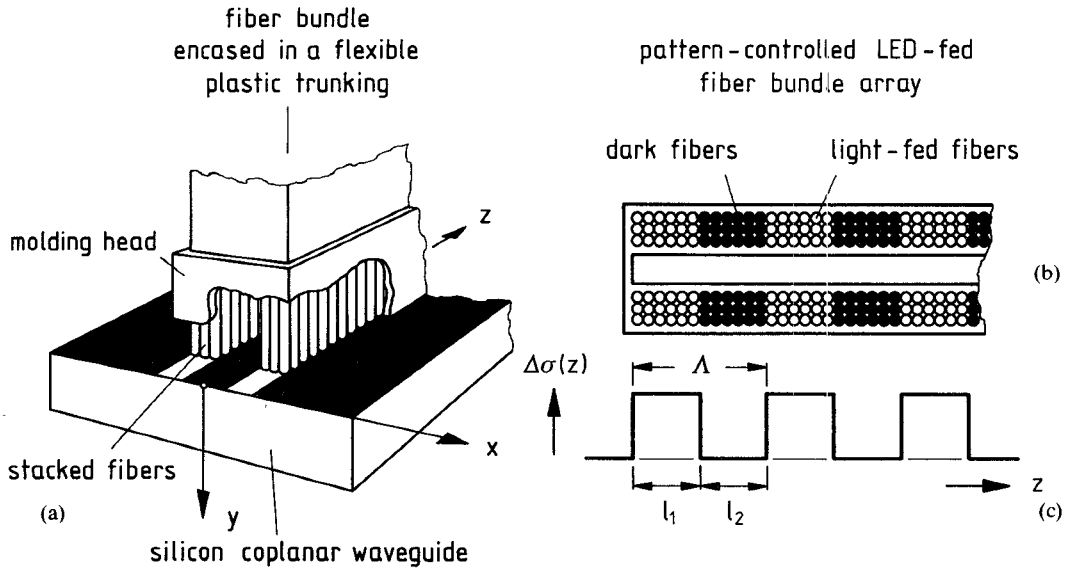

Fig. 11. Sketch of the prototype of coplanar PPS on silicon substrate illuminated by a pattern-controlled LED-fed fiber bundle array on top of the CPW: (a) total configuration with cutaway section of the molding head; (b) cross-sectional view of the molding head; and (c) induced longitudinal profile of photoconductivity $\Delta\sigma(z)$

where $Z_p(z)$ is obtained from (7) by using $\Delta\vartheta_e(z) = (q_\epsilon q_p \Delta\sigma_e/\omega\epsilon_0\epsilon_{re})\cdot\rho(z)$ along with $\rho(z)$ from (10). In the reference plane (RP) at $z=0$ (Fig. 2), the contribution to the total input reflection coefficient Γ_{ss-0} of a single excited section from this step is

$$d\Gamma_0(z) = d\Gamma(z)\exp\left\{-2\int_0^z [\alpha(\zeta)+j\beta(\zeta)]\,d\zeta\right\} \quad \text{(A2)}$$

where ζ is a dummy variable introduced for the integration. A second integration finally yields

$$\Gamma_{ss-0} = \int_0^\infty d\Gamma_0(z). \quad \text{(A3)}$$

Considering that $\rho(z)$ is given in the trisection analytical form of (10), Γ_{ss-0} can be presented as the sum of the separated subsection reflection coefficients Γ_{IN-0}, Γ_{H-0}, and Γ_{OUT-0} according to (11). Owing to the need for transforming the inner reflection coefficients $\Gamma_H(z=l_0)$ and $\Gamma_{OUT}(z=l_0+l_1)$ into the reference plane at $z=0$, one obtains

$$\Gamma_{IN-0} = \int_0^{l_0}\left[d\Gamma_{IN}(z)\exp\left\{-2\int_0^z[\alpha_{IN}(\zeta)+j\beta]\,d\zeta\right\}\right] \quad \text{(A4a)}$$

$$\Gamma_{H-0} = \exp\left\{-2\int_0^{l_0}[\alpha_{IN}(z)+j\beta]\,dz\right\}\cdot\int_{l_0}^{l_0+l_1}\left[d\Gamma_H(z)\exp\left\{-2\int_{l_0}^z[\alpha_H(\zeta)+j\beta]\,d\zeta\right\}\right] \quad \text{(A4b)}$$

$$\Gamma_{OUT-0} = \exp\left\{-2\int_0^{l_0}[\alpha_{IN}(z)+j\beta]\,dz - 2\int_{l_0}^{l_0+l_1}[\alpha_H(z)+j\beta]\,dz\right\}\cdot\int_{l_0+l_1}^{2l_0+l_1}\left[d\Gamma_{OUT}(z)\cdot\exp\left\{-2\int_{l_0+l_1}^z[\alpha_{OUT}(\zeta)+j\beta]\,d\zeta\right\}\right] \quad \text{(A4c)}$$

where $\beta=\beta_l$ and is assumed to be independent of z according to (6). As relevant carrier diffusion occurs only within the distance $l_0 \simeq 4L_a$, it is sufficient in practice to integrate from $z_1=0$ to $z_2=2l_0+l_1$ instead of $z_2=\infty$.

After having performed the straightforward integration of the exponential terms along with some algebraic manipulation, (A4) can be rewritten as

$$\Gamma_{IN-0} = \frac{jN\exp M}{4L_a}\int_0^{l_0}\frac{\exp[Dz - M\exp(z/L_a) - j2Bz]}{1-jN\exp(z/L_a)}\,dz \quad \text{(A5a)}$$

$$\Gamma_{H-0} = -\frac{jAV\exp(M+2Al_0)}{2BL_a}\int_{l_0}^{l_0+l_1}\frac{E(z)\exp[-2(\alpha_0+A)z+2AVE(z)L_a - j2Bz]}{1-jNC^{-1}[1-VF(z)]}\,dz \quad \text{(A5b)}$$

$$\Gamma_{OUT-0} = -\frac{jN\exp(M-2Al_1)}{4U^2L_a}\int_{l_0+l_1}^{2l_0+l_1}\frac{\exp[-(2\alpha_0+L_a^{-1})z + MU^{-2}\exp(-z/L_a) - j2Bz]}{1-jNU^{-2}\exp(-z/L_a)}\,dz \quad \text{(A5c)}$$

with the following notations: $A=\beta_l\Delta\vartheta_e/2$; $B=\beta_l$; $C=\sinh(l_1/2L_a)\exp(-l_0/L_a - l_1/2L_a)$; $D=L_a^{-1}-2\alpha_0$; $E(z)=\sinh(z/L_a - l_0/L_a - l_1/2L_a)$; $F(z)=\cosh(z/L_a - l_0/L_a - l_1/2L_a)$; $M=2ACL_a$; $N=2ACB^{-1}$; $U=\exp(-l_0/L_a - l_1/2L_a)$; $V=\exp(-l_1/2L_a)$; and $\alpha_0=\alpha_\epsilon+\alpha_d$.

ACKNOWLEDGMENT

This paper is dedicated to Prof. Dr.-Ing. H. H. Brand (Erlangen, West Germany) on the occasion of his 60th birthday. The author would like to thank A. Harth, who

carried out the numerical integrations, and B. Schmauss for performing the measurements.

REFERENCES

[1] C. H. Lee, Ed., *Picosecond Optoelectronic Devices*. London: Academic Press, 1984.

[2] W. Platte, "Optoelectronic microwave switching," in *Proc. Military Microwaves Conf.* (London), 1984, pp. 276–286; also *Proc. Inst. Elec. Eng.*, pt. J., vol. 132, pp. 126–132, 1985.

[3] G. L. Matthaei, L. Young, and E. M. T. Jones, *Microwave Filters, Impedance-Matching Networks, and Coupling Structures*. New York: McGraw-Hill, 1964.

[4] R. E. Collin, *Foundations for Microwave Engineering*. New York: McGraw-Hill, 1966, pp. 224–254.

[5] W. Platte, "Optical control of microwaves by LED-induced DBR structures in silicon coplanar waveguides," *Electron. Lett.*, vol. 25, pp. 177–179, 1989.

[6] M. Matsumoto, M. Tsutsumi, and N. Kumagai, "Bragg reflection characteristics of millimeter waves in a periodically plasma-induced semiconductor waveguide," *IEEE Trans. Microwave Theory Tech.*, vol. MTT-34, pp. 406–411, 1986.

[7] W. Platte, "Optoelectronic microwave switching via laser-induced plasma tapers in GaAs microstrip sections," *IEEE Trans. Microwave Theory Tech.*, vol. MTT-29, pp. 1010–1018, 1981.

[8] K. C. Gupta, R. Garg, and I. J. Bahl, *Microstrip Lines and Slotlines*. Dedham, MA: Artech House, 1979.

[9] W. Platte and B. Sauerer, "Optically CW-induced losses in semiconductor coplanar waveguides." *IEEE Trans. Microwave Theory Tech.*, vol. 37, pp. 139–149, 1989.

[10] W. Platte, "Effective photoconductivity and plasma depth in optically quasi-CW controlled microwave switching devices," *Proc. Inst. Elec. Eng.*, pt. J., vol. 135, pp. 251–254, 1988.

[11] W. Platte, "Longitudinal conductivity profile in periodically photoexcited semiconductor transmission lines," *Proc. Inst. Elec. Eng.*, pt. J., vol. 136, pp. 108–110, 1989.

[12] W. Platte, "Switched optoelectronic microwave load," *Proc. Inst. Elec. Eng.*, pt. I., vol. 129, pp. 193–198, 1982.

[13] A. Harth and W. Platte, Internal Rep. IHFT-ST 476, Univ. Erlangen-Nuernberg, Erlangen, West Germany, 1988.

[14] W. Platte, "Photoinduced microwave attenuation in LED-controlled semiconductor coplanar waveguides," *Arch. Elek. Übertragung.*, vol. 42, pp. 322–325, 1988.

[15] B. Schmauss and W. Platte, Internal Rep. IHFT-DA 490, Univ. Erlangen-Nuernberg, Erlangen, West Germany, 1989.

[16] W. Platte and W. Renz, "Measurement of small optically pulse-modulated reflection coefficients," *Electron. Lett.*, vol. 19, pp. 625–627, 1983.

✠

Walter Platte was born in Remscheid-Lennep, West Germany, on January 24, 1943. He received the Dipl.-Ing. degree in electrical engineering from the Technical University of Aachen, Aachen, West Germany, in 1968 and the Dr.-Ing. degree in electrical engineering and the Habilitation degree ("venia legendi") from the University of Erlangen-Nuernberg, Erlangen, West Germany, in 1975 and 1986, respectively.

From 1968 to 1969, he worked at AEG-Telefunken, Ulm, West Germany, on *Ku*-band radar instrumentation and measurement, in particular Doppler radar moving target simulators. Since October 1969, he has been with the Department of High-Frequency Techniques, University of Erlangen-Nuernberg, where he is engaged in research on laser-controlled MIC and millimeter wave components, optoelectronics, optical communications, and fiber sensors. In addition, he has been lecturing on optical communication devices at the University of Erlangen-Nuernberg since 1977. In 1986, he was made an Adjunct Staff Member (Privat-Dozent) in the Faculty of Engineering Sciences at the university.

Dr. Platte is a member of the Verband Deutscher Elektrotechniker (VDE/NTG). He was awarded the Annual Prize of the Nachrichtentechnische Gesellschaft (NTG) in 1977 and the Finkelnburg-Habilitation Prize of the University of Erlangen-Nuernberg in 1987.